



# Rheological and mechanical properties of mortars prepared with natural and manufactured sands

D.D. Cortes<sup>a</sup>, H.-K. Kim<sup>b,\*</sup>, A.M. Palomino<sup>c</sup>, J.C. Santamarina<sup>a</sup>

<sup>a</sup> Georgia Institute of Technology, Atlanta, GA, USA

<sup>b</sup> Kookmin University, Seoul, South Korea

<sup>c</sup> Department of Civil Engineering, Penn State University, PA, USA

## ARTICLE INFO

### Article history:

Received 7 August 2006

Accepted 25 March 2008

### Keywords:

Aggregate

Mortar

Compressive strength

Mixture proportioning

## ABSTRACT

The conventional assessment methods for fine aggregate used in Portland cement concrete are mostly based on round natural sand performance in spite of the increasing use of angular manufactured sands. Two natural and two manufactured sands were selected and tested at different water–cement ratios and fine aggregate-to-cement ratios for the same standard gradation to identify shape-related differences on the mechanical performance of mortars. Three tests were used in this study: flowability, stiffness and strength. Results showed that adequate flow and compressive strength were attained when the volume of paste exceeded the volume of voids in the loosely packed aggregate, i.e., just above the maximum void ratio  $e_{\max}$  of the fine aggregate. Given the dependence of  $e_{\max}$  on particle shape, mixture predesign can be facilitated by taking aggregate shape into consideration.

© 2008 Elsevier Ltd. All rights reserved.

## 1. Introduction

The formation history of sands determines their particle shape. Natural sands tend to be round due to the cumulative effect of multiple collisions and abrasion. Manufactured sands are the product of rock crushing, which creates grains with distinctive particle shapes that depend on the parent rock composition, fracture mode, coordination number during crushing, and the reduction ratio. The crushing process tends to produce angular, sharp edged particles. Rough angular particles yield a granular packing of lower density, lower small strain stiffness, and higher critical state friction angle when compared with more rounded natural sands [1].

The shape and texture of crushed sand particles could lead to improvements in the strength of concrete due to better interlocking between particles [2]. However, angular fine aggregate produces mortar of lower workability than spherical sands for the same water content [3–5], or the same volume of cement paste [5–7]. Additional water is often incorporated into cement mixtures to improve workability, yet higher water content decreases strength, even though the angular particles themselves increase interparticle shear resistance [8].

The use of angular manufactured sands in Portland cement concrete has significantly increased over the last 25 years, especially in areas where natural sands are scarce. Despite the wider

use of manufactured sands, current aggregate quality assessment methods are primarily based on round natural sand performance. Specifications for concrete sand invariably consider grain size distribution; other requirements may include sand equivalency, durability, organic impurities, fineness modulus, and reactivity. Even though the sand from a particular source meets all these requirements, there is no guarantee that the sand will perform satisfactorily in concrete. Other sand characteristics such as mineralogy, particle shape, and surface texture are not necessarily measured by typical tests. Yet, they may strongly influence overall performance [3].

The purpose of this study was to conduct a systematic comparison of the effects natural and manufacture sands exert on mortar properties. We present first the results of a detailed characterization of the selected fine aggregates, followed by the flow behavior of fresh mortars, and both P-wave velocity and compressive strength of hardened mortars. Note that coarse aggregate was not included in the tested mixtures.

## 2. Experimental design

### 2.1. Material description

Four different sands were selected for this study, two natural sands and two manufactured sands: (1) Georgia Department of Transportation GDOT standard cement sand (from Butler, GA), (2) mixture of natural silica sands (coarser grains >0.3 mm, from Junction City, GA; finer grains ≤0.3 mm, from Ottawa F110), (3) crushed granite sand (from Fayette, GA), and (4) crushed limestone sand (from Floyd, GA).

\* Corresponding author. Tel.: +82 2 910 4692.

E-mail address: [geotech@kookmin.ac.kr](mailto:geotech@kookmin.ac.kr) (H.-K. Kim).

The four sands were sieved to obtain the same grain size distribution shown as a dotted line in Fig. 1. The recommended grain size distribution range for the standard concrete sand – 10NS of the GDOT supplemental specification section 801 – is represented by the shaded area in Fig. 1. Measured index properties of the tested sands are summarized in Table 1.

Quartz is the prevailing mineral in both natural sands (more than 99% by mass). The crushed granite sand consists of ~90% quartz or feldspar minerals (microcline, plagioclase) and ~5–10% mica (biotite, muscovite) by mass. These mica particles are smaller than 300  $\mu\text{m}$  in size. The crushed limestone sand is mostly  $\text{CaCO}_3$  (hardness index 3).

The roundness and sphericity of 90 sand grains were measured for each sand using optical microscopy (Leica M26 Stereomicroscope) and the Krumbein and Sloss classification chart [9]. Selected images are assembled in Fig. 2. The shape factors for mean size  $D_{50}$  particles of all observed sands fell within a narrow range (Table 1); the finer  $D_{90}$  particles were distinctively more angular and platier in manufactured sands than in natural sands. Furthermore, optical microscopy images revealed that crushed granite sand had sharper edges than crushed limestone sand.

The angle of repose was obtained from side-view digital images of sand piles, while the maximum and minimum void ratios  $e_{\text{max}}$  and  $e_{\text{min}}$  were determined following standard ASTM procedures [10,11].

## 2.2. Test procedures

A total of 64 mortar batches (Portland cement type I–II, water, and fine aggregate) were prepared by mixing each of the four sand specimens at four water–cement ratios:  $w/c=0.42, 0.46, 0.50,$  and  $0.54,$  and at four fine aggregate to cement ratios:  $\text{FA}/c=2.00, 2.75, 3.25,$  and  $4.00.$  Mass-blending fractions for all mixes are shown in Table 2. Admixtures were not incorporated.

Three tests were conducted for each mixture. The flow test was run on the fresh mortar. Small-strain P-wave velocity and large-strain unconfined compressive strength were run on seven-day hardened mortar cubes.

The flow test was performed following the ASTM standard [12]. A cone-shaped mold was placed on the center of a vibrating table and filled with freshly mixed hydraulic cement mortar in two lifts. When the mold was removed, the vibrating table was dropped 25 times in 15 s. Flow is the percentage increase in mortar diameter. We captured the horizontal spread of the mortar pile using digital photography

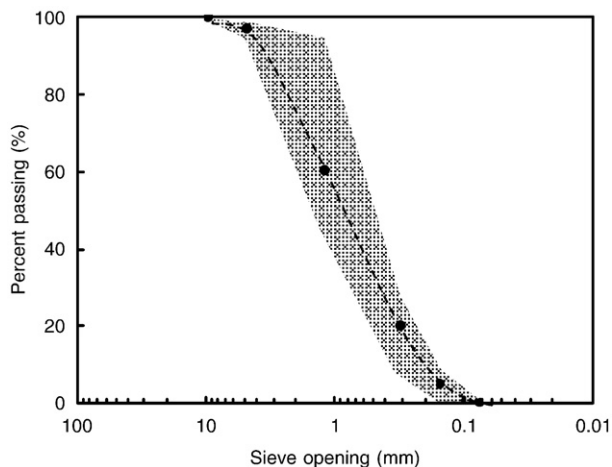


Fig. 1. Grain size distribution of selected sands. (The dotted line is the same for the four tested sands.) The shaded area represents the GDOT target band for standard concrete sand (10NS).

Table 1  
Engineering properties of tested sands

Sand	Sphericity	Roundness	$e_{\text{max}}$	$e_{\text{min}}$	Angle of repose
GDOT standard	0.71	0.39	0.73	0.43	36°
Mixed natural	0.71	0.42	0.72	0.43	35°
Crushed granite	0.62	0.27	0.75	0.43	38°
Crushed limestone	0.64	0.33	0.77	0.44	37°

Note: The shape parameters are based on measurements of 90 grains. The variation in sphericity and roundness is about  $\pm 0.15$ .

during 25 drops. The physical meaning of the flow test was previously reported by the authors [13].

Each mortar batch provided enough material for three cubical specimens. Cubes were prepared by filling the cubical molds with two layers and tamping 32 times per layer, and cured in airtight containers for seven days, as described in the ASTM standard [14]. The P-wave velocity of the seven-day cured specimens was determined using P-wave piezocrystals (MATEC CSO.0510, 50 kHz) and peripheral electronics. Finally, the unconfined compressive strength was measured by recording the applied peak axial force during uniaxial compression of the mortar cubes.

## 3. Experimental results

### 3.1. Fresh mortar flowability

Images of mortar spread after 25 drops are presented in a mosaic format that parallels the test matrix (Fig. 3). The case shown in Fig. 3 corresponds to mixtures prepared with the GDOT standard sand. “Wet-flow” is herein used to designate mortars that show a continuous slurry surface. In contrast, “dry-flow” designates mortars that break and spread in granulated form. Table 3 summarizes the flow data for all mixtures following a table organization that parallels the picture mosaic in Fig. 3. The boundary that separates the visual distinction between wet-flow (shaded cells in Table 3) and dry-flow is shown in each case. Clearly, mixtures exhibited wet-flow when  $w/c$  was high and  $\text{FA}/c$  was low. Note that a large flow radius was also obtained with high  $\text{FA}/c$  and low  $w/c$  mixtures under dry-flow conditions.

### 3.2. Small strain P-wave velocity

Table 4 summarizes the mean P-wave velocity for the specimens prepared with each mixture. At low  $w/c$  and  $\text{FA}/c \geq 2.75$ , the measured mortar mixture P-wave velocity varied significantly with aggregate type, i.e. natural and manufactured sands. However, when  $w/c$  was high and  $\text{FA}/c$  was low, the difference in the P-wave velocity became less pronounced. Specimens with internal heterogeneity can yield poor first arrivals due to multiple travel paths, and the measured P-wave velocities are less reliable; such cases are denoted with an asterisk in Table 4: they fall in the dry-flow region, i.e., more difficult to compaction.

### 3.3. Unconfined compressive strength

Unconfined compressive strength data are summarized versus  $\text{FA}/c$  and  $w/c$  for all sands in Table 5. Higher strength values were measured on specimens that exhibited wet-flow conditions.

### 3.4. General observations

Flow, P-wave velocity and compressive strength trends can be misleading when the data in Tables 3, 4 or 5 are plotted versus either  $\text{FA}/c$  or  $w/c$  because trends reverse across the dry-flow to wet-flow

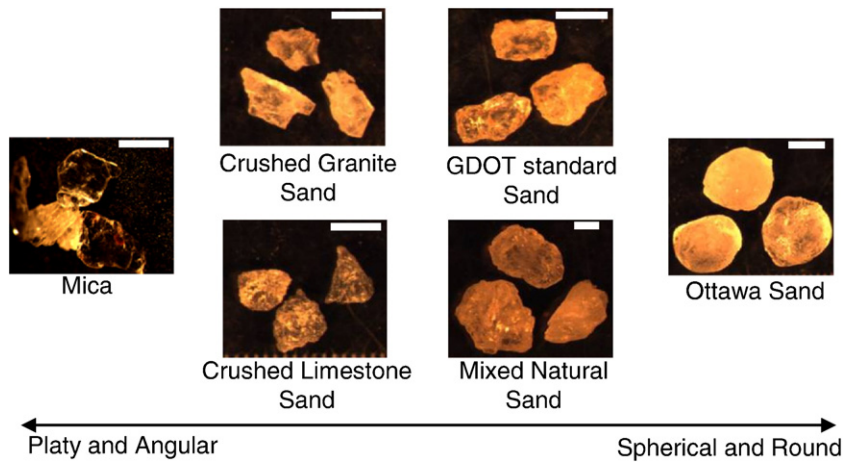


Fig. 2. Optical microscopy pictures of sand particles. The length of white segments is 0.5 mm in all pictures.

transition. A detailed volumetric–mechanical interpretation is attempted next.

4. Analysis and discussion

4.1. Particle shape and packing density

Sphericity and roundness reveal aspects of the particle formation history and play a major role in determining the bulk behavior of the aggregate. Shape irregularities limit particle mobility and their ability to attain minimum potential energy in tightly packed configurations. As a result, the maximum void ratio,  $e_{max}$ , the minimum void ratio,  $e_{min}$ , and the difference  $I_e = e_{max} - e_{min}$  increase as the particles become more angular and irregular. While the tested sands comprised a limited range in particle shape, results in Table 1 are in agreement with published trends [1], and differences in frictional resistance and packing density among the sands reflect differences in particle shape.

4.2. Flow and volume fraction of paste  $V_p/V_{FA}$

The transition from dry-flow to wet-flow can be analyzed in terms of the ratio between the volume of cement paste  $V_p$  and the volume of solids in the fine aggregate  $V_{FA}$ . The volume fraction  $V_p/V_{FA}$  can be expressed in terms of the specific gravity  $G$ , unit weight  $\gamma$ , and the weight  $W$  of each component:

$$\frac{V_p}{V_{FA}} = \frac{(V_c + V_w)}{V_{FA}} = \frac{\frac{W_c}{\gamma_w G_c} + \frac{W_w}{\gamma_w}}{\frac{W_{FA}}{\gamma_w G_{FA}}} = \frac{W_c \cdot (1/G_c + w/c)}{W_{FA}/G_{FA}} = \frac{G_{FA} \cdot (1/G_c + w/c)}{(FA/c)} \tag{1}$$

where the subscripts stand for  $w$ : water,  $c$ : cement, and  $FA$ : fine aggregate. The ratio  $w/c$  is water–cement ratio, and  $FA/c$  is fine aggregate to cement ratio.

Flow is plotted versus  $V_p/V_{FA}$  in Fig. 4 ( $G_{FA} = 2.6\text{--}2.7$ , measured for each sand;  $G_c = 3.12$ ). Mixtures that exhibit wet-flow conditions are

identified as encircled points. Under saturated conditions (approximation in wet-flow mixtures), the volume fraction  $V_p/V_{FA}$  is equivalent to the void ratio in the fine aggregate. For comparison, we identify the two extreme void ratios  $e_{max}$  and  $e_{min}$  for each sand in Fig. 4. It can be concluded that wet-flow is attained when sufficient paste is available to separate the grains beyond the loosest packing density of the sand  $e_{max}$  so that the interaction between sand grains is minimized. A graphical interpretation is presented in Fig. 5.

Results in Fig. 4 suggest a minimum amount of paste  $V_p/V_{FA} = 1.1 \pm 0.05 e_{max}$  to attain wet-flow in specimens prepared with either natural or manufactured sands. As manufactured sands pack at higher values of  $e_{max}$ , more paste will be required for manufactured sand mortars to attain the same flowability as the natural sand mortars.

4.3. Flow and strength

Strength data are plotted versus flow in Fig. 6, where wet-flow mixtures are distinguished by encircling data points. In the dry-flow regime, mortar spreads in granulated form, without conserving volume; spreading increases at low  $V_p/V_{FA}$ . Capillary forces hinder densification and together with the insufficient volume of paste result in air pockets inside the hardened mortar, and reduced strength. Thus, there is negative correlation between measured flow values and the corresponding compressive strengths for all dry-flow mixtures (Fig. 6).

In the wet-flow regime ( $V_p/V_{FA} > \sim 1.1 e_{max}$ ), the mortar compressive strength is controlled by the water–cement ratio of the paste (Fig. 6). A positive correlation between flow and strength is observed only in a narrow range of  $FA/c$  near the transition from dry-flow to wet-flow (Fig. 6). Strength may decrease in high flow mixtures at high  $V_p/V_{FA}$ . The envelopes sketched on Fig. 6 capture these observations.

4.4. Strength and stiffness

P-wave velocity is plotted versus compressive strength in Fig. 7 (Note: similar trends were found in previous studies [15,16]).

Table 2  
Tested mortars – identical ratios are used with each of the four fine aggregates

Batch ID	1	2	3	4	5	6	7	8	9	10	11	12	13	14	15	16
Water [%]	12.3	13.3	14.3	15.3	10.1	10.9	11.8	12.6	9.0	9.8	10.5	11.3	7.7	8.4	9.1	9.7
Cement [%]	29.2	28.9	28.6	28.2	24.0	23.8	23.5	23.3	21.4	21.2	21.1	20.9	18.5	18.3	18.2	18.1
Aggregate [%]	58.5	57.8	57.1	56.5	65.9	65.3	64.7	64.1	69.6	69.0	68.4	67.8	73.8	73.3	72.7	72.2

Note: Values are mass fractions.

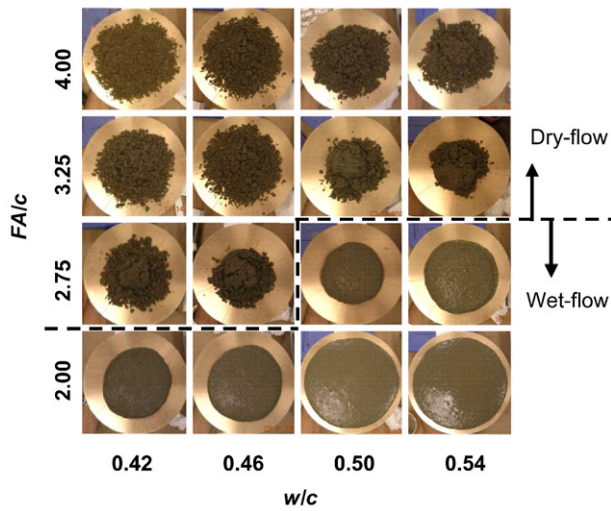


Fig. 3. Flow at 25 drops. These mortars are prepared with Georgia DOT standard concrete sand. The dotted line indicates the boundary between “wet-flow” and “dry-flow”.

Velocity and strength are positively correlated when the compressive strength is below ~15 MPa (only dry-flow mixtures are found in this region). Thereafter, the volume fraction of paste  $V_P/V_{FA}$  and the  $w/c$  ratio have a pronounced effect on strength, as they control porosity and pore size distribution. However,  $V_P/V_{FA}$ ,  $w/c$  or even sand type (shape and mineralogy) have almost no effect on the P-wave velocity of hardened wet-flow mixtures within the resolution of the gathered data (Fig. 7); apparently, the properties of fine aggregates are concealed by the properties of the paste that fills

Table 4  
P-wave velocity: The effect of fine aggregate-to-cement FA/c and water-to-cement w/c ratios on the small-strain stiffness of 7-day cured mortars

GDOT standard sand mortars					Mixed natural sand mortars						
FA/c	4.00	3.1	3.5	3.5	3.4	FA/c	4.00	3.0	3.4	3.4	3.7
	3.25	3.5	3.9	3.8	3.7		3.25	3.6	3.7	3.7	3.6
	2.75	3.9	3.9	3.7	3.6		2.75	3.8	3.7	3.6	3.6
	2.00	3.8	3.6	3.5	3.5		2.00	3.6	3.6	3.6	3.5
		0.42	0.46	0.50	0.54			0.42	0.46	0.50	0.54
	w/c					w/c					
Crushed granite sand mortars					Crushed limestone sand mortars						
FA/c	4.00	1.7*	2.2	1.7	3.2	FA/c	4.00	3.0	3.2	3.6	3.7
	3.25	2.6	1.3*	3.3	3.6		3.25	3.0	3.3	3.9	4.0
	2.75	2.7	1.4*	3.7	3.7		2.75	3.4	4.0	3.9	3.7
	2.00	3.8	3.5	3.4	4.1		2.00	3.9	3.8	3.7	3.6
		0.42	0.46	0.50	0.54			0.42	0.46	0.50	0.54
	w/c					w/c					

Note: The asterisk indicates weak first arrivals. Values of P-wave velocity are expressed in km/s.

the voids, and the asymptotic P-wave velocity is determined by the mortar.

5. Conclusions

We implemented a comprehensive experimental study of mortars prepared with two round natural sands and two angular

Table 3  
Flow: The effect of fine aggregate-to-cement FA/c and water-cement w/c ratios on fresh mortar flowability

GDOT standard sand mortars					Mixed natural sand mortars						
FA/c	4.00	78	57	36	31	FA/c	4.00	81	68	64	52
	3.25	63	34	36	64		3.25	69	43	24	36
	2.75	54	72	109	114		2.75	35	38	57	93
	2.00	38	90	120	128		2.00	72	98	116	135
		0.42	0.46	0.50	0.54			0.42	0.46	0.50	0.54
	w/c					w/c					
Crushed granite sand mortars					Crushed limestone sand mortars						
FA/c	4.00	105	96	88	59	FA/c	4.00	95	83	58	69
	3.25	99	83	52	52		3.25	99	78	42	37
	2.75	70	67	46	46		2.75	90	44	38	82
	2.00	37	83	99	110		2.00	38	90	120	128
		0.42	0.46	0.50	0.54			0.42	0.46	0.50	0.54
	w/c					w/c					

Flow  $F$  is defined as  $F=(R_{25}-R_0)/R_0 \times 100[\%]$ , where  $R_{25}$  is the radius of the mortar pile after the 25th drop and  $R_0$  is the initial radius of the mortar pile (ASTM C 1437 2001).

Table 5  
Unconfined compressive strength: The effect of fine aggregate-to-cement FA/c and water-cement w/c ratios on uniaxial compression strength of 7-day cured mortars

GDOT standard sand mortars					Mixed natural sand mortars						
FA/c	4.00	4.0	8.8	9.1	7.8	FA/c	4.00	5.5	10	9.9	7.4
	3.25	12	20	16	19		3.25	9.7	21	24	24
	2.75	24	28	32	30		2.75	27	20	32	34
	2.00	43	41	32	30		2.00	38	38	37	34
		0.42	0.46	0.50	0.54			0.42	0.46	0.50	0.54
	w/c					w/c					
Crushed granite sand mortars					Crushed limestone sand mortars						
FA/c	4.00	1.0	0.9	0.6	4.9	FA/c	4.00	3.2	5.0	12	10
	3.25	1.5	3.4	6.4	9.7		3.25	3.4	6.4	20	30
	2.75	3.5	5.3	29	21		2.75	5.7	28	38	31
	2.00	23	38	33	32		2.00	44	46	38	34
		0.42	0.46	0.50	0.54			0.42	0.46	0.50	0.54
	w/c					w/c					

Values of compressive strength expressed in MPa.

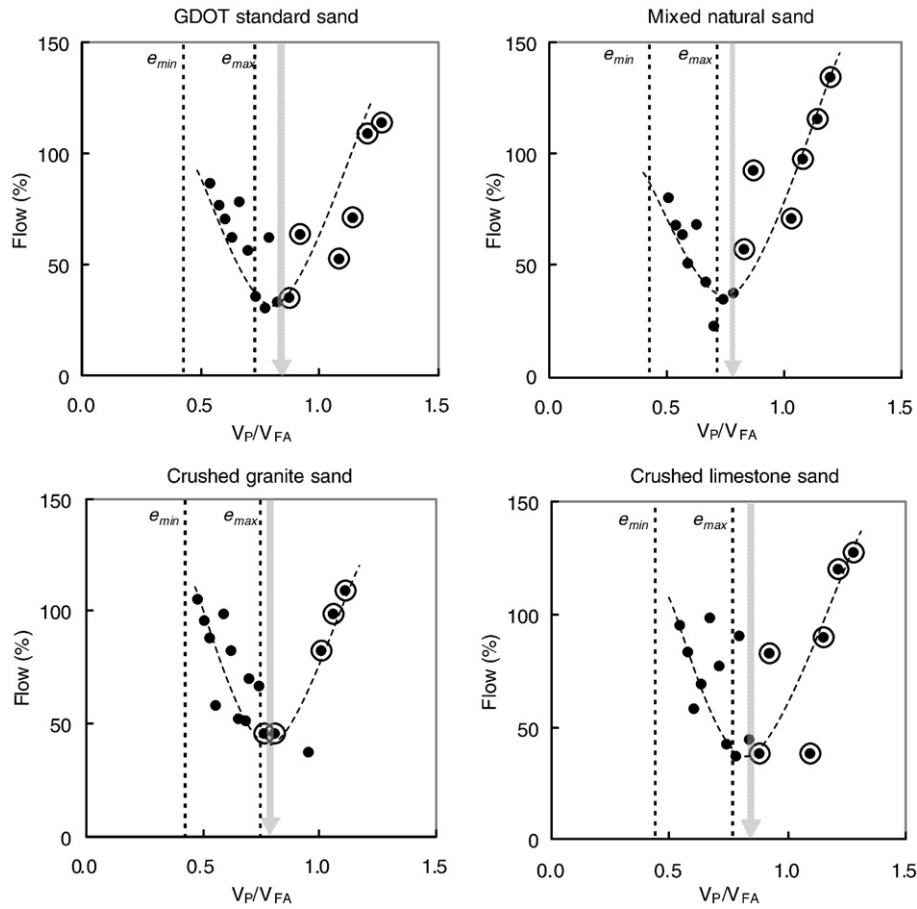


**Fig. 4.** Flow vs. relative volume of cement paste  $V_p/V_{FA}$ . Wetness is visually assessed from digital image mosaics similar to the one shown in Fig. 3. The arrows indicate the boundary between dry-flow and wet-flow. Encircled data points indicate specimens that exhibit wet-flow.

manufactured sands, at various water–cement and fine aggregate–cement ratios to evaluate the roles of particle shape on flow, P-wave velocity, and unconfined compressive strength. Conclusions follow:

- Mortars exhibit “wet-flow” (i.e., keep a continuous slurry-type surface while flowing) when the volume of paste  $V_p$  is greater than the volume of voids within the loosely packed fine aggregate  $V_{FA}$ . The boundary is found at  $V_p/V_{FA} > \sim 1.1 e_{max}$  in the tested sands.
- Flow and the volume fraction of cement paste  $V_p/V_{FA}$  are negatively correlated in the dry-flow regime ( $V_p/V_{FA} < \sim 1.1 e_{max}$ ) as mortars spread in granular form. The positive correlation between flow and  $V_p/V_{FA}$  in wet-flow mixtures ( $V_p/V_{FA} > \sim 1.1 e_{max}$ ) reflects reduced interaction between sand grains.
- The unconfined compressive strength and flow are positively correlated near the  $V_p/V_{FA} > \sim 1.1 e_{max}$  transition. Thereafter, strength reaches an asymptote value or may even decrease at high paste

volume fraction. The asymptotic strength depends on the paste w/c, rather than on the type of fine aggregate.

- The small-strain stiffness of hardened wet-flow mortars is controlled by the paste stiffness, as the paste fills the voids and conceals the properties of grains (shape and mineralogy) on small-strain measurements.
- The loosest packing density of the fine aggregate  $e_{max}$  depends on particle shape. Therefore, a larger volume of paste will be required to attain adequate flowability and strength when angular crushed fine aggregates are used instead of natural round aggregates of the same grain size distribution.

**Acknowledgements**

This research was supported by a grant from the Georgia Department of Transportation and the Georgia Construction

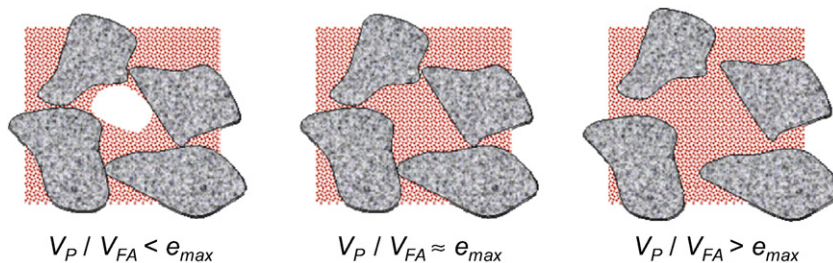


**Fig. 5.** Volume fraction between the volume of cement paste  $V_p$  and the volume of solids in the fine aggregate  $V_{FA}$ .

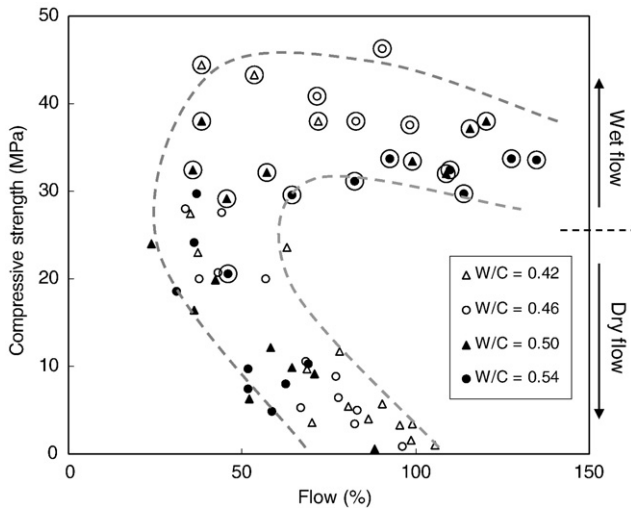


**Fig. 6.** Fresh mortar flow vs. 7-day compressive strength for all tested sands. Encircled data points indicate specimens that exhibit wet-flow.

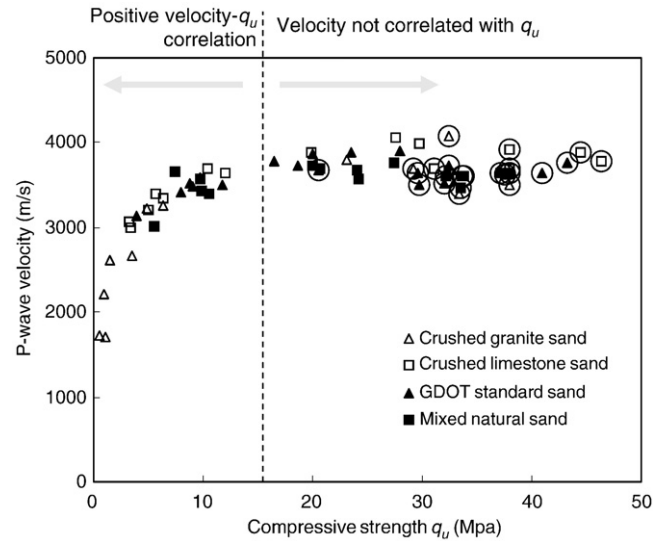


**Fig. 7.** Compressive strength versus P-wave velocity (7-day cured cement mortars). Encircled data points indicate specimens that exhibit wet-flow.

Aggregate Association (GCAA). Additional support was provided by the Goizueta Foundation.

## References

- [1] G.C. Cho, J.S. Dodds, J.C. Santamarina, Particle shape effects on packing density, stiffness and strength – natural and crushed sands, *ASCE Journal of Geotechnical and Geoenvironmental Engineering* 132 (5) (2006) 591–602.
- [2] H. Donza, O. Cabrera, E.F. Irassar, High-strength concrete with different fine aggregate, *Cement and Concrete Research* 32 (11) (2002) 1755–1761.
- [3] P. Quiroga, D. Fowler, The effects of aggregates characteristics on the performance of portland cement concrete, *International Center for Aggregates Research* 104-1F (2004) 358.
- [4] S. Jamkar, C. Rao, Index of aggregate particle shape and texture of coarse aggregate as a parameter for concrete mix proportioning, *Cement and Concrete Research* 34 (11) (2004) 2021–2027.
- [5] M. Westerholm, Rheology of the mortar phase of concrete with crushed aggregate, Department of Chemical Engineering and Geosciences, Licentiate, vol. 198, Luleå University of Technology, Stockholm, 2006.
- [6] F.I. Mel'nikov, Use of calculation methods for determining compositions of refractory concretes, *Refractories and Industrial Ceramics* 11 (1970) 591–595.
- [7] H. Järvenpää, Quality characteristics of fine aggregates and controlling their effects on concrete, Department of Materials Science and Rock Engineering, Helsinki University of Technology, Doctor of Technology, vol. 243, 2001.
- [8] M.F. Kaplan, Flexural and compressive strength of concrete as affected by the properties of coarse aggregates, *American Concrete Institute* 55 (1959) 1193–1208.
- [9] W.C. Krumbein, L.L. Sloss, Stratigraphy and sedimentation, W.H. Freeman and Company, San Francisco, 1963, p. 497.
- [10] ASTM D 4253-00 "Standard Test Methods for Maximum Index Density and Unit Weight of Soils Using a Vibratory Table." American Society for Testing and Materials.
- [11] ASTM D 4254-00 "Standard Test Methods for Minimum Index Density and Unit Weight of Soils and Calculation of Relative Density." American Society for Testing and Materials.
- [12] ASTM C1437-01 "Standard Test Method for Flow of Hydraulic Cement Mortar." American Society for Testing and Materials.
- [13] H.K. Kim, D.D. Cortes, J.C. Santamarina, Flow test: particle-level and macroscale analyses, *ACI Materials Journal* 104 (3) (2007) 323–327.
- [14] ASTM C 109 "Standard Test Method for Compressive Strength of Hydraulic Cement Mortars." American Society for Testing and Materials.
- [15] R. Jones, E.N. Gatfield, Testing concrete by an ultrasonic pulse technique, *Road Research Technical* 34 (1955) 48.
- [16] D.F. Orchard, *Concrete Technology*, Applied Science Publisher Ltd., London, 1979, p. 375.